Available online at www.sciencedirect.com

SciVerse ScienceDirect

Energy Procedia 00 (2014) 000–000

Energy Procedia

www.elsevier.com/locate/procedia

SHC 2013, International Conference on Solar Heating and Cooling for Buildings and Industry
September 23-25, 2013, Freiburg, Germany

BiPV system performance and efficiency drops: overview on PV module temperature conditions of different module types

Laura Maturi[a]*, Giorgio Belluardo[a], David Moser[a], Matteo Del Buono[a]

[a]*EURAC, Viale Druso 1, Bolzano 39100, Italy*
**tel.: +39-0471-055633; fax: +39-0471-055699; e-mail: laura.maturi@eurac.edu*

Abstract

A typical problem of BiPV systems (Building Integrated Photovoltaic) is the power loss due to temperature increase, because modules often operate close to the building envelope with low ventilation.
It is thus essential to properly evaluate and compare the PV temperature conditions of different PV module categories (in terms of PV technology and material type). Several explicit correlations exist for the evaluation of the PV module temperature, among which the simplest and most handy is a linear expression (i.e. $T_{mod}=T_{amb}+k\ G$) which links T_{mod} with the ambient temperature (T_{amb}) and the incident solar radiation flux (G).
Within this expression the value of the dimensional parameter k, known as the Ross coefficient, depends on several aspects (i.e. module type, wind velocity and integration characteristics).
However, dispersed values for this parameter can be found in literature (in the range of 0.02-0.06 K m^2/W) according to different module types, while more information are provided regarding different integration characteristics.
This paper aims at giving an overview of the value of k for different module types according to monitored data registered over one year time period at the ABD-PV plant in Bolzano (Italy).
The highest values of k, which means the highest module temperature at a certain G, are registered for the three glass-glass (G-G) module types ($k_{Tmod,c}$ from 0.033 K m^2/W to 0.037 K m^2/W). The glass-tedlar (G-T) module types operate at slight lower temperature values ($k_{Tmod,c}$ ranging from 0.029 K m^2/W to 0.032 K m^2/W).

Selection and peer review by the scientific conference committee of SHC 2013 under responsibility of PSE AG.

Building Integrated Photovoltaic; BiPV; PV temperature; PV modules; PV outdoor monitoring

Selection and peer review by the scientific conference committee of SHC 2013 under responsibility of PSE AG.

1. Introduction

A typical problem of BiPV systems (Building Integrated Photovoltaic) is the power loss due to temperature increase, because modules often operate close to the building envelope with low ventilation (Nordmann and Clavadetscher, 2003 [1]) (Trinuruk et al., 2009 [2]) (Maturi et al., 2012 [3]). The operating temperature in fact plays a central role in the photovoltaic conversion process, as well as on the electrical efficiency and, hence, the power output of a PV module depends practically linearly but rather strongly on T_{mod}, decreasing with it [4]. It is thus essential to properly evaluate the module temperature profile for different PV working conditions.

Several explicit correlations exist for the evaluation of PV module temperature [2,4,5,6,7,8], among which the simplest is a linear expression (i.e. $T_{mod}=T_{amb}+k\ G$) which links T_{mod} with the ambient temperature (T_{amb}) and the incident solar radiation (G).

This paper aims at giving an overview of the values of k for different module categories according to monitored data registered over one year time period (August 2012 – July 2013) at the ABD-PV plant in Bolzano (Italy) allowing to evaluate and compare PV module temperatures of different module types.

Nomenclature

m-Si	mono crystalline
a-Si	amorphous silicon
IR	infrared
ΔT_{max}	maximum temperature gradient within the PV module (among four points)
T_{mod}	PV module temperature
$T_{mod,avg}$	back of module temperature average of four points of the module back side
$T_{mod,c}$	back of module temperature in the center of the module back side
T_{amb}	ambient temperature
k	Ross coefficient
R^2	coefficient of determination
RMSE	root-mean-square error
G-G	glass-glass PV module type
G-G_{bs}	glass-glass PV module type, with a black sheet in the back side
G-T	glass-tedlar PV module type
WF	PV module with frame
NF	PV module without frame
v_{wind}	wind velocity
G	irradiance
G_{STC}	irradiance under Standard Test Conditions
P_n	array nominal power
PR	array performance ratio

2. Experimental set-up

The modules investigated are listed on an anonymous basis in Table 1.

The six monitored modules are installed on a rack with a fixed inclination of 30° (grid connected system) almost facing South, located in the ABD-PV plant of the airport “Aeroporto Bolzano Dolomiti” in Bolzano (North of Italy), which is in operation since August 2010. The European Academy of Bozen/Bolzano (EURAC) is the scientific responsible for monitoring the performance of the ABD-PV plant (Colli et al. [10]). Electric and production data regarding PV modules are recorded automatically by the inverters with a frequency of 15 minutes, while the PV back of module temperature is recorded every minute by means of temperature sensors (Pt100) attached on the back

side of the modules. The weather data are recorded every minute with the support of a meteo station which is located in the ABD-PV plant area and averaged over a 15-minutes time interval. It is equipped with sensors for the measurement of irradiance on horizontal and module plane, ambient temperature, wind speed and direction. The acquisition system and measurement errors are described in details by Fanni et al [11].

Table 1. List of investigated modules

nr.	name	technology	Stratigraphy	Frame
1	CIGS3	CIGS	glass-glass (G-G)	WF
2	mc-Si4	m-Si-back contact	glass-tedlar (G-T)	WF
3	mc-Si3	m-Si	glass-tedlar (G-T)	WF
4	mc-Si1	m-Si	glass-glass (G-G)	NF
5	mc-Si2	m-Si	glass-glass-black sheet (G-G_{bs})	NF
6	1j-a-Si2	a-Si	glass-tedlar (G-T)	WF

Figure 1 shows the monitored PV arrays: all modules considered for the analysis in this paper are installed close to each other, in identical conditions (i.e. tilt angle 30°, azimuth 8.5° West of South, rack mounted).

The back of module temperature values are acquired with a Pt100 attached in the center of the back side of the module located in the middle of each array. The global irradiance is measured with a pyranometer (Kipp & Zonen CMP) at tilt of 30° (same plane as the modules). The ambient temperature (T_{amb}) is acquired with a Pt100 which is covered by a weather and radiation protection shield. The wind velocity and direction are measured with a sonic anemometer. All weather data are logged with one minute time resolution and average on 15-minutes time intervals.

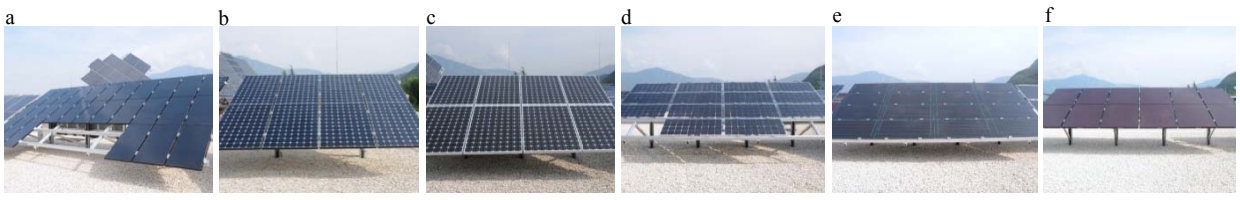

Figure 1: arrays of the six monitored PV modules. (a) CIGS3, (b) mc-Si4, (c) mc-Si3, (d) mc-Si1, (e) mc-Si2, (f) 1j-a-Si2

3. Methodology

3.1. Thermography measurements

The thermography technique is used for a preliminary evaluation of the back-side temperature distribution of each module.

Thermography measurements were performed at a sunny cloudless day, with the module working at mppt, with an angle view higher than 60° to the module glass and setting the right emissivity depending on the module type.

The IR-image of the mc-Si2 module in Figure 2 (a) shows a temperature gradient within the panel up to 7.1°C along line 1 as displayed in Figure 2 (b). In this case, the temperature peak is reached in the middle of the module: the lateral parts are significantly cooler, due to the absence of the metal frame. The same temperature distribution, i.e. with a significant temperature increase in the middle, is observed for the other module without frame (i.e. mc-Si1 module). The other modules, which have a metal frame (i.e. CIGS3, mc-Si4, mc-Si3, 1j-a-Si2), present a more homogeneous temperature distribution within the module. Figure 3 shows the typical temperature distribution of a module with frame: in this case, the temperature gradient along line 1 is 2.5°C.

a b

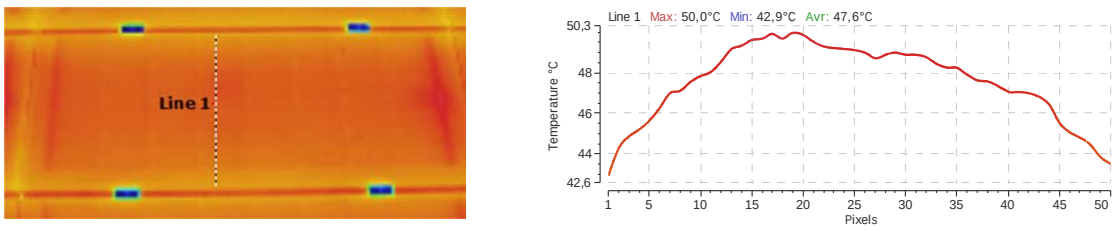

Figure 2: (a) IR-image of the mc-Si2 module, (b) temperature distribution referred to line 1 of the IR-image shown in (a)

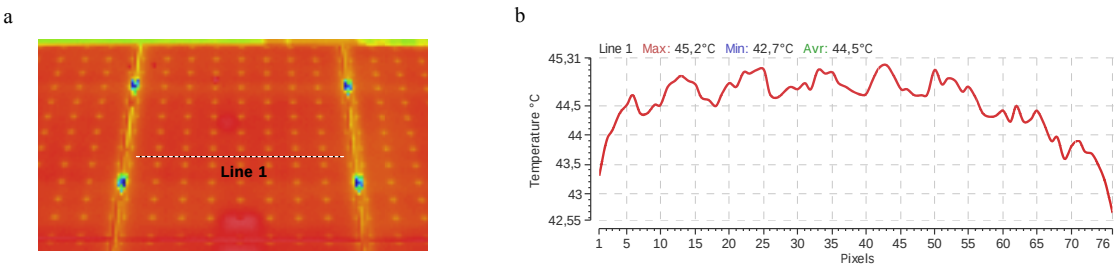

Figure 3: (a) IR-image of the mc-Si4 module, (b) temperature distribution referred to line 1 of the IR-image shown in (a)

3.2. Additional temperature measurements

In order to better evaluate the amplitude of the temperature gradient within the panel over different conditions, additional measurements are carried out by means of a portable thermometer with four thermocouples.

The back side temperature is thus measured for at least three sunny days, in four points of each module (i.e. in the center, in the corner and in the two lateral sides, as indicated in the IEC 60891 [12]).

The maximum registered temperature gradient (ΔT_{max}) is reported in Table 2 for each module. The temperature gradient ΔT_{max} is defined as the difference between the max and min values among the four measured points.

Values of ΔT_{max} range from 4.5°C to 6.3°C for modules with frame. Similar values are reported in other studies (i.e. [13,14]) that report temperature gradient within framed modules of about 3°C-5°C.

For the two modules without frame (i.e. mc-Si1 and mc-si2), measured values of ΔT_{max} exceed 8°C. These data confirm the trend shown in the thermography measurements, where the highest ΔT_{max} is displayed for the modules without frame.

Table 2. values of ΔT_{max} for each module (i.e. maximum temperature gradient within the PV module among four measured points). Framed modules in bold

nr.	**1**	**2**	**3**	4	5	**6**
ΔT_{max} [°C]	**4.5**	**5.7**	**6.1**	8.0	8.8	**6.3**

3.3. Temperature data

The Pt100 sensor is attached in the center of the modules back side, and thus a complete data-set on temperature values over a whole year is available just for the modules central point.

On the other hand, paragraphs 3.1and 3.2 show that there could be a significant temperature gradient within a single module, especially if it is without frame. Consequently, the temperature measured in one single point could not be representative of the module temperature.

For this reason we also used the additional data measured in four points (as specified in paragraph 3.2) to calibrate the acquired temperature values.

The spatial average temperature measured in the four points ($T_{mod,avg}$) is plotted against the temperature measured in the center of each module $T_{mod,c}$ and the calibration coefficients are evaluated through a linear regression, according to the following equation:

$$T_{mod,avg} = a + b * T_{mod,c} \tag{1}$$

The resulting coefficients *a* and *b* are reported in Table 3 for each module.

Table 3. calibration coefficients *a* and *b* referred to equation (1) and coefficient of determination related to each linear regression. Framed modules in bold

nr.	**1**	**2**	**3**	4	5	**6**
a	**0.583**	**0.507**	**0.247**	1.318	1.350	**-0.042**
b	**0.983**	**0.976**	**1.004**	0.943	0.948	**1.011**
R^2	**0.998**	**0.998**	**0.998**	0.998	0.999	**0.997**

3.4. Filtering procedure

A filtering is performed on the 15-minutes data before calculating the Ross coefficient *k*. The first filter exclude points corresponding to a ratio of diffuse and global irradiance higher than 0.20 in order to consider just clear sky conditions, i.e. conditions in which the direct irradiance component is predominant on the diffuse one.

A second filter considers points as valid only within the range $PR_{avg}\pm\sigma$, where:

- PR_{avg} is the average value of performance ratio of the PV array for the considered period, defined by the international standard IEC 61724 [15] as:

$$PR = \frac{E}{P_n}\frac{G_{STC}}{G}$$

  where E is the energy production (Wh), P_n the array nominal power (W) and G_{STC} the irradiance under STC conditions (1000 W/m^2)
- σ is the standard deviation

In this way, outlier points are excluded which correspond to situations in which the *PR* is too high or too low, respectively due to irradiance on the module larger than the one measured by pyranometer, and irradiance on the module lower than the one measured by pyranometer. This condition may occur with a not-uniform cloud cover or shadowing due to obstacles, such as mountains, and is more evident the longer is the distance between module and irradiance sensor.

Finally, points corresponding to morning time are filtered out. The reason for this can be seen in Figure 4, which represents $T_{mod,avg}$-T_{amb} against irradiance after applying the two previously described filters. Points related to glass-glass modules (as for example mc-Si2) show a different trend depending on the time of the day. A lower curve is clearly visible, which correspond to points measured in the morning (approximately before 1 PM). During this period of the day, the glass-glass module seem to be affected by thermal inertia: the module heats up due to increasing ambient temperature and irradiance, but the back of the module temperature does not increase simultaneously, lagging up to 5 degrees behind the cell temperature until thermal equilibrium is reached . The same effect occurs also during the afternoon when the module cools down but in a minor extent, and the linearity of $T_{mod,avg}$-T_{amb} with G is less affected.

Thermal inertia has been observed by different authors [16,17], and it seems to occur also on glass-tedlar module (see Figure 4a), but is less visible. Its effect on different module types will be deeper analyzed in a future study.

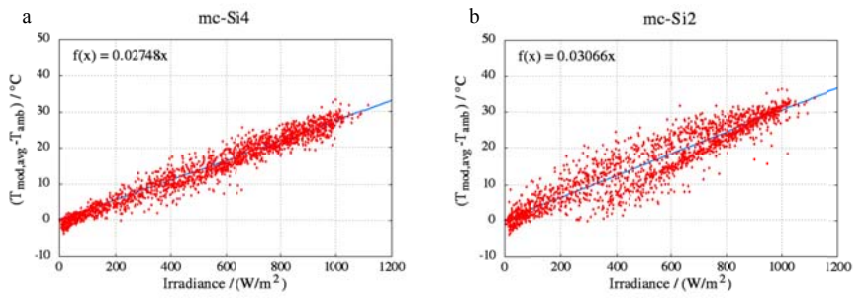

Figure 4: Plots of $T_{mod,avg}$-T_{amb} against irradiance for a) a glass-tedlar module type b) a glass-glass module type; ratio of diffuse to global irradiance and $PR_{avg}\pm\sigma$ filters applied

4. Results

4.1. Ross coefficients overview

The values of $T_{mod,avg}$-T_{amb} are plotted against irradiance for each module type (see Figure 5). The plotted values refer to data filtered according to the procedure described in paragraph 3.4, with the additional filter 0.9 m/s<v_{wind}<1.1m/s.

The least-squares-fit line through the set of data is evaluated with an additional constraint, such as $T_{mod,avg}$-T_{amb}=0˚C when G=0 W/m^2, for the physical meaning related to the thermal equilibrium, in steady state conditions, when no irradiance is present. The Ross coefficient k is evaluated as the slope of that line.

Table 4 provides an overview of the evaluated k values, which are valid for wind velocities of 1m/s (±0.1m/s). $k_{Tmod,c}$ is defined as the Ross coefficient evaluated plotting temperature data measured just in the back side module center; $k_{Tmod,avg}$ is defined as the Ross coefficient evaluated plotting "calibrated" temperature data which take into account also peripheral values, by applying the coefficients presented in paragraph 3.3. In the last columns, $k_{Tmod,avg,Garc.}$ is also reported, which corresponds to $k_{Tmod,avg}$ calculated taking into account points filtered as described in paragraph 3.4, with the only difference of excluding values of G<800W/m^2 instead of values measured in the morning, according to the observations of Alonso García and Balenzategui [17].

The difference between $k_{Tmod,c}$ and $k_{Tmod,avg}$ is negligible for WF module types, while it becomes slightly higher for NF module types. This finding is in agreement with results shown in paragraphs 3.1 and 3.2, showing that the highest ΔT_{max} occurs for the NF modules and the highest back-side temperature values are registered in the module center. In fact, the values of $k_{Tmod,avg}$ takes into consideration also peripheral module temperature values, which are highly influenced not only by the stratigraphy of the module, but also by the absence of the frame (see module temperature distribution of a NF module in Figure 2). In general the values of $k_{Tmod,avg,Garc.}$ are slightly lower than $k_{Tmod,avg}$, but result in the same trend.

In order to compare the PV back of module temperature of different modules stratigraphy, the least-squares-fit lines of each module type, according to the values of $k_{Tmod,c}$ of Table 4 , are plotted in Figure 5.

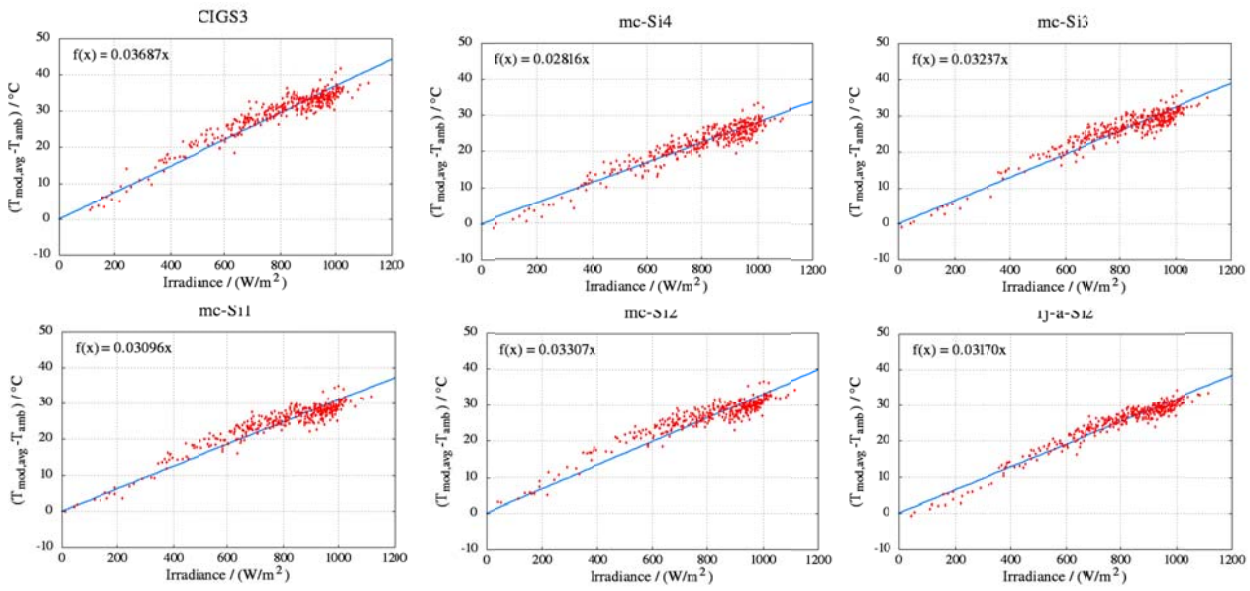

Figure 5: Plots of $T_{mod,avg}$-T_{amb} against irradiance for each module type; all filters applied

By considering the back of module temperature $T_{mod,c}$, the highest PV temperatures at a certain irradiance G correspond to the three glass-glass (G-G) module types (see Figure 6). For these module types the value of $k_{Tmod,c}$ ranges from 0.033 K m^2/W to 0.037 K m^2/W (see red lines in Figure 5). The glass-tedlar (G-T) module types operate at slight lower temperature values, with $k_{Tmod,c}$ ranging from 0.029 K m^2/W to 0.032 K m^2/W (see blue lines in Figure 5). For example, according to the evaluated $k_{Tmod,c}$, in conditions of irradiance of 1000W/m^2 and air velocity of 1m/s, the warmest module (i.e. CIGS3) operates at a temperature which is 8°C higher than the coolest one (i.e. mc-Si4), possibly affecting the PV power production up to 3% (e.g. considering a temperature coefficient of 0.36%/°C for CIGS3 and of 0.38%/°C for mc-Si4).

Table 4. Ross coefficient k overview evaluated experimentally

nr.	name	technology	Stratigraphy	Frame	$k_{Tmod,c}$ (K m^2/W)	$RMSE_{k\_Tmod,c}$	$k_{Tmod,avg}$ (K m^2/W)	$RMSE_{k\_Tmod,avg}$	$k_{Tmod,avg,Garc.}$ (K m^2/W)	$RMSE_{k\_Tmod,avg,Garc.}$
1	CIGS3	CIGS	glass-glass (G-G)	WF	0.037	2.3	0.037	2.4	0.036	2.1
2	mc-Si4	m-Si-back contact	glass-tedlar (G-T)	WF	0.029	2.0	0.028	2.1	0.028	1.9
3	mc-Si3	m-Si	glass-tedlar (G-T)	WF	0.032	2.2	0.032	2.2	0.031	1.9
4	mc-Si1	m-Si	glass-glass (G-G)	NF	0.033	2.0	0.031	2.2	0.030	1.9
5	mc-Si2	m-Si	glass-glass-black sheet (G-G_{bs})	NF	0.035	2.4	0.033	2.5	0.031	2.0
6	1j-a-Si2	a-Si	glass-tedlar (G-T)	WF	0.031	1.7	0.032	1.6	0.031	1.5

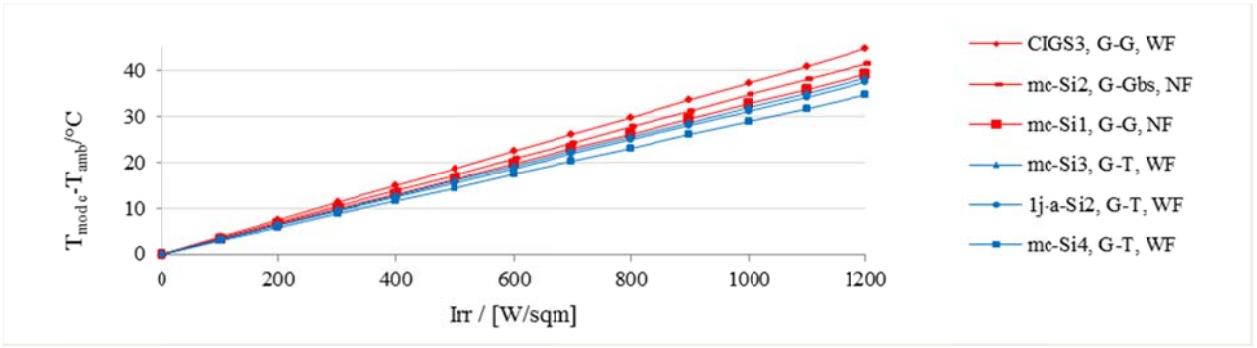

Figure 6: Plots of the least-squares-fit lines of each module type, according to the $k_{Tmod,c}$ values

4.2. Wind dependence of Ross coefficient

The results presented above, refer to a constant wind velocity of 1m/s (±0.1m/s). Anyway, the wind velocity could have a strong influence on the *k* parameter [4].

A correlation between *k* and the wind velocity is thus evaluated for each module type, by plotting the *k* values (i.e. $(T_{mod,avg}-T_{amb})/G$), against wind velocity using experimental data filtered according to the procedure discussed in paragraph 3.4.

The experimental correlation found for each module type, in agreement with earlier studies [4,18,19], is in the form:

$$k(v_{wind}) = a + b * \exp(-c * v_{wind}) \tag{2}$$

In Figure 7, the plots of *k* (i.e. $(T_{mod,avg}-T_{amb})/G$), against wind velocity for each module type are presented.

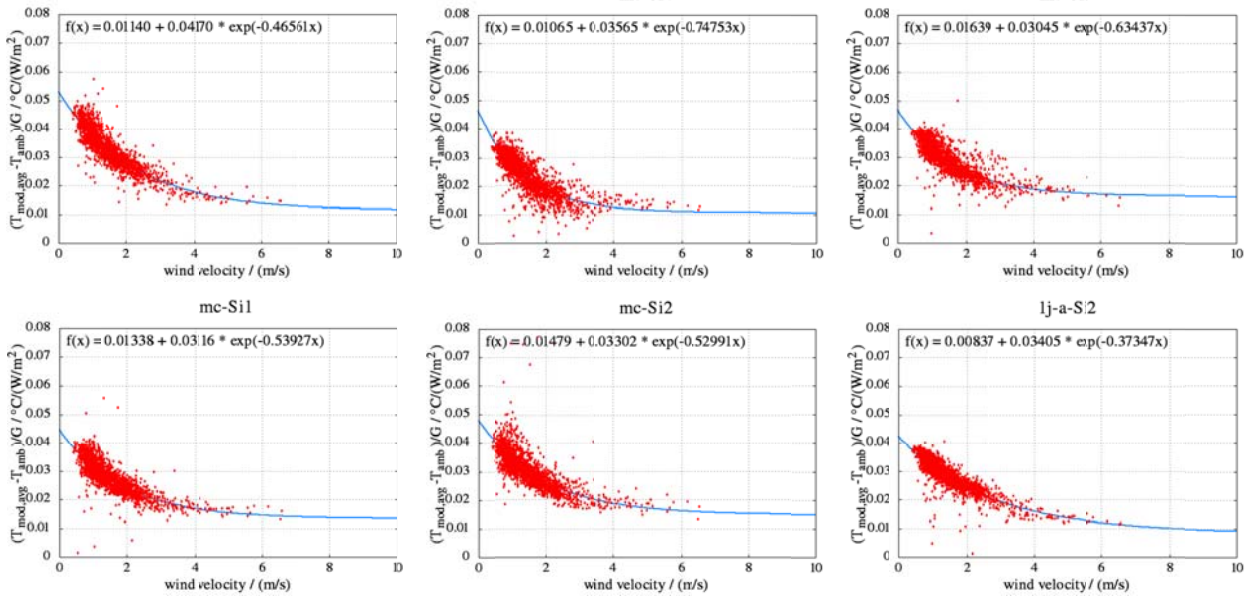

Figure 7: Plots of *k* (i.e. $(T_{mod,avg}-T_{amb})/G$), against wind velocity for each module type

The experimental coefficients *a*, *b* and *c* referred to equation (2), are summarized in Table 5. As expected, results obtained from this equation for v_{wind}=1, are in good agreement with the ones presented in paragraph 4.1.

Table 5. experimental coefficients *a*, *b* and *c* for each module type, referred to the formula (2)

nr.	name	technology	Stratigraphy	Frame	a	b	c	RMSE
1	CIGS3	CIGS	glass-glass (G-G)	WF	0.011	0.042	0.466	0.0033
2	mc-Si4	m-Si-back contact	glass-tedlar (G-T)	WF	0.011	0.036	0.748	0.0035
3	mc-Si3	m-Si	glass-tedlar (G-T)	WF	0.016	0.030	0.634	0.0031
4	mc-Si1	m-Si	glass-glass (G-G)	NF	0.013	0.031	0.539	0.0032
5	mc-Si2	m-Si	glass-glass-black sheet (G-G_{bs})	NF	0.015	0.033	0.530	0.0040
6	1j-a-Si2	a-Si	glass-tedlar (G-T)	WF	0.008	0.034	0.373	0.0026

5. Conclusions

In this paper an overview of *k* values evaluated experimentally for six module types is provided and a wind dependence of *k* has been introduced.

The main conclusions follow:

- The highest values of *k*, which means the highest back of the module temperature at a certain G, is given by the three glass-glass (G-G) module types ($k_{Tmod,c}$ from 0.033 K m^2/W to 0.037 K m^2/W). The glass-tedlar (G-T) module types operate at slight lower temperature values ($k_{Tmod,c}$ ranging from 0.029 K m^2/W to 0.032 K m^2/W).
- The thermography measurements show that the NF modules present a temperature gradient within the panel (around 7.1°C) quite higher compared to the WF modules (around 2.5°C). This behavior is confirmed by other measurements carried out with 4 temperature sensors placed in 4 points of the module back side, which report a ΔT_{max} from 4.5°C to 6.3°C for WF modules and ΔT_{max} exceeding 8°C for NF modules. This could be due to the fact that lateral parts of the NF modules are significantly cooler, due to the absence of the metal frame. Consequently, temperature values measured in one central point of the module could be considered as representative of the average operating temperature for WF modules while, for NF modules, it could be significantly different.
- The role of the module thermal inertia should be taken into consideration when analyzing module back-side temperature data. As the thermal inertia of G-G modules is higher than the one of G-T modules, the effect of thermal inertia is more visible for these type of modules.

Acknowledgements

The authors would like to thank the fund EFRE-Provincia Autonoma di Bolzano Alto Adige (Fondo Europeo di sviluppo regionale) for the financial contribution through the project 2-la-97 “PV-Initiative”, as well as the European Union for funding the project n.310220 "On-the-fly alterable thin-film solar modules for design driven applications" within the Seventh Framework Programme.

Reference

[1] Nordmann T, Clavadetscher L. Understanding temperature effects on PV system performance. Proceedings of 3rd World Conference on Photovoltaic Energy Conversion, 2003, Vol. 3, p. 2243 –2246.

[2] Trinuruk P, Sorapipatana C, Chenvidhya D. Estimating operating cell temperature of BIPV modules in Thailand. Renewable Energy, 2009, Vol. 34, 2515–2523.

[3] Maturi L et al. BiPV façade systems: effectiveness of a passive strategy to improve the PV performance. Proceedings of the 27th European Photovoltaic Solar Energy Conference, 2012, p. 4203 – 4206.
[4] Skoplaki E, Boudouvis AG, Palyvos JA. A simple correlation for the operating temperature of photovoltaic modules of arbitrary mounting. Solar Energy Materials and Solar Cells. 2008 Nov, Vol. 92, p.1393–1402.
[5] Skoplaki E, Palyvos JA. Operating temperature of photovoltaic modules: A survey of pertinent correlations. Renewable Energy, 2009, Vol. 34, p. 23–29.
[6] Chenni R et al. A detailed modeling method for photovoltaic cells. Energy, 2007, Vol. 32, p.1724–1730.
[7] Risser VV, Fuentes MK. Linear regression analysis of flatplate photovoltaic system performance data. Proceedings of the 5th E.C. photovoltaic solar energy conference, 1983, p. 623–627.
[8] Servant JM, 1985. Calculation of the cell temperature for photovoltaic modules from climatic data. Proceedings of the 9th biennial congress of ISES – Intersol 85, Montreal, Canada, extended abstracts, p. 370.
[9] Ross RG, Smokler MI. Flat-plate solar array project final report-VolVI: Engineering Sciences and reliability. Report DOE/JLP-1012-125, 1986.
[10] Colli A et al., 2010. Performance monitoring of different PV technologies at a PV field in Northern Italy. Proceedings of the 25th European Photovoltaic Solar Energy Conference and Exhibition / 5th World Conference on Photovoltaic Energy Conversion, 2010, p. 4344 – 4349.
[11] Fanni L et al. How accurate is a commercial monitoring system for photovoltaic plant?. Progress in Photovoltaics: Research and Applications, 2012.
[12] International Standard IEC 60891, 2009-12. Photovoltaic devices – Procedures for temperature and irradiance corrections to measured I-V characteristics.
[13] Buerhop C, Scheuerpflug H, Weissmann R. The role of infrared emissivity of glass on IR-Imaging of PV-plants. Proceedings of the 26th European Photovoltaic Solar Energy Conference 2011; 3413 – 3416.
[14] Lee Y, Tay AAO. Finite element thermal analysis of a solar photovoltaic module. Energy Procedia 2012;15;413-420.
[15] International Standard IEC 61724, 1998. Photovoltaic System Performance monitoring – Guidelines for Measurement, Data Exchange, and Analysis.
[16] King DL, Boyson WE, Kratochvill JA. Photovoltaic array performance model. Sandia Report SAND2004-3535, 2004.
[17] Alonso García MC, Balenzategui JL. Estimation of photovoltaic module yearly temperature and performance based on Nominal Operation Cell Temperature calculations. Renewable Energy, Vol. 29, 2004, p. 1997-2010.
[18] Kurnik J, Jankovec M, Brecl K, Topic M. Outdoor testing of PV module temperature and performance under different mounting and operational conditions. Solar Energy Materials and Solar Cells. 2011, Vol. 95, p. 373–376.
[19] Hart GW, Raghuraman P. Simulation of thermal aspects of residential photovoltaic systems. MIT Report DOE/ET/20279-202, 1982.